2012

Preferentially Orienting Ag Nanoparticles Using CaF2 Nanorods

Mathias Auer
Virginia Commonwealth University

Preferentially Orienting Ag nanoparticles using CaF2 nanorods

A thesis submitted in partial fulfillment of the requirements for the degree of Master of

Science in Physics / Applied Physics at Virginia Commonwealth University.

By

Mathias Auer

B.S. in Physics

Virginia Commonwealth University, 2010

M.S. in Physics/Applied Physics

Virginia Commonwealth University, 2012

Director:

Dexian Ye, Assistant Professor, Department of Physics

Virginia Commonwealth University

Richmond, Virginia, 23284

May, 2012

Acknowledgments

Above all, I would like to thank my mother for ensuring that I would always have what I needed to seek any educational path I desired. I would like to thank my father for being my first mentor in the physical sciences, and my sister for always believing in me even when my faith in myself was not the strongest.

To properly express my gratitude to the numerous faculty members in the VCU physics department who have contributed to my education would require a thesis sized work in itself. In the limited space that I am provided here I would like to thank every teacher and faculty member in the department, for the countless hours they have spent in the classroom and the office aiding me in my academics and research. I would like to especially thank Dr. Dexian Ye for his guidance as my graduate academic advisor and for pushing me to seek out opportunities for myself that seemed unreachable to me at the time. To say that this study was made possible in part due to Dr. Massimo Bertino and Louis Franzel would be an understatement of astronomical proportions. Thank you both for all of the work done that was far above the call of obligation. I would also like to thank Dr. Dimitry Pestov for all of his help in this work as well. Finally, thank you Dr. Alison Baski for providing me with this opportunity by offering me a GTA position.

Lastly, I would like to thank my friends for providing me with sanity and stability when I needed it the most, and for putting up with me when sanity was not attainable. In the physics department I would like to thank Sean, Chuck, Louis, Steele, Mike, Vince, Roy, and Sue. Outside of the department a big thank you goes to Bill, Paul, Grayson, Tom, Mary, Justine, Eliza, Nathan, Gina, Mike, and Justin. You are the people who have made my college years as fun as they were. Once again, thank you VCU physics!

Table of Contents

List of Figures

Abstract

Preferentially Orienting Ag nanoparticles using CaF2 nanorods

By Mathias L. Auer

A thesis submitted in partial fulfillment of the requirements of the degree of Master of Science at Virginia Commonwealth University. Virginia Commonwealth University, 2012.

Major Director: Dr. Dexian Ye, Assistant Professor, Department of Physics

A study was done to examine the effect of surface orientation as well as heterogeneous epitaxy at an interface between two materials with a large lattice mismatch. Silver nanoparticles of different diameters were grown in an effort to study methods of preferentially orienting the geometry of metal nanoparticles. Arrays of calcium fluoride nanorods were grown on silicon substrates using oblique angle thermal vapor deposition. The chamber operated at an ultra high vacuum pressure of 1×10^{-10} Torr during the deposition of the rods and an oblique angle of 75° was kept between the silicon substrate normal and the direction of incident flux. A method was then developed to grow silver nanoparticles exclusively on the (111) facet of the calcium fluoride tips. This was accomplished by once again using oblique angle deposition with an angle of 75° along with the larger size of the (111) calcium fluoride tip facet. Cross sectional

scanning electron microscopy and transmission electron microscopy imaging was used to verify that the nanoparticles adhered exclusively to the desired facet of the tip. Using selected area diffraction, (SAED) and dark field in the TEM, it was shown that the nanoparticles did grow at a (111) orientation at the interface between them and the calcium fluoride rods. Different thicknesses and diameters of nanoparticles were then grown to determine what an ideal size was to achieve the most (111) orientation of the nanoparticles. Thicknesses of the particles varied between 5 nanometers and 15 nanometers. Through characterization it was shown that all three of the different thicknesses grown exhibited (111) orientation of the silver nanoparticles, both at the interface and in the overall nanoparticle as well with the 10 nanometer sample being the most ideal in terms of the desired result. Lattice straining of the silver nanoparticles was also observed by characterization through diffraction and SAED.

Chapter 1: Motivation and Literature Review

1.1 Catalysis

In a chemical reaction, a catalyst is a substance that changes the rate of the reaction without being consumed by the reaction itself. [1] Catalysts can be used to either speed up or slow down the rate of a chemical reaction. A vast majority of industrial chemicals and biochemically significant processes (approximately 90 percent) use catalysts or are "catalyzed". [2] Catalysts play a very important role in industrial chemical production as well as many other aspects of life in that they can drastically improve the efficiency of the reaction by reducing the time and waste of a reaction. Catalytic reactions also have significant environmental advantages by reducing the level of waste (toxic or otherwise) in industrial chemical production (as opposed to traditional stoichiometric reactions in which all reactants are consumed and more side products are formed). Catalysts can be a useful tool for converting hazardous or harmful waste into more benign products such as the catalytic converter in the internal combustion engine. [3] Transition metals are often used as catalysts.

Generally, Catalysts react with one or more reactants to form intermediates that will in turn yield the final reaction product, which regenerates the catalyst in the process. [1] This is done by the catalyst providing an alternative reaction pathway to the reaction product. This increases the rate of the reaction as the alternative route has the

lower activation energy. Using X and Y to represent the reactants, C to represent the catalyst and Z as the product of the reaction, a typical catalytic reaction scheme can be represented as follows:

$$X + C \rightarrow XC \tag{1}$$
$$Y + XC \rightarrow XYC \tag{2}$$
$$XYC \rightarrow CZ \tag{3}$$
$$CZ \rightarrow C + Z. \tag{4}$$

In this instance, the catalyst is consumed by reaction 1 and produced in reaction 4 which makes the overall reaction, [1]

$$X + Y \rightarrow Z. \tag{5}$$

In recent years, the design of catalysts at the nanoscale has attracted a lot of interest due to the increased ability to control structures and geometries. [4] This in turn has lead to the optimization and specialization of catalysts which in turn saves time, money, and resources. It has been a goal to obtain a greater fundamental insight into the features of nanoscale catalysts that influence the activity, selectivity, and lifetime of nanocatalysts so as to make better and more efficient ones. Nanocatalysis has yielded some novel catalytic properties such as greatly enhanced reactivity and selectivity of transition metals as nanoparticles as compared to their bulk material. [3] Particle size has proven to be a definitive factor with regards to catalytic activity. However, other factors such as geometry, composition, oxidation state, and chemical/physical environment can play roles in the reactivity of the nanoparticles as well. [3] The more that is understood about these nano-size dependent effects that are not exhibited or at least are not exhibited as

strongly in the bulk, the more easily we can exploit these properties to a multitude of advantages in science and industry. This work is an effort to further the understanding of metal nanoparticle catalytic properties to attain better control and specialization of these properties.

1.2 Calcium fluoride nanorods

Using extreme shadowing growth techniques also known as oblique angle deposition, it is possible to grow biaxially textured films of isolated nanostructures on amorphous substrates or substrates at relatively ambient temperatures. [5,6,7] The growth of calcium fluoride films consisting of biaxial tipped nanorods, as shown in Fig 1.1 has been demonstrated recently by Li *et al.* along with some novel properties characteristic of these structures. [7]
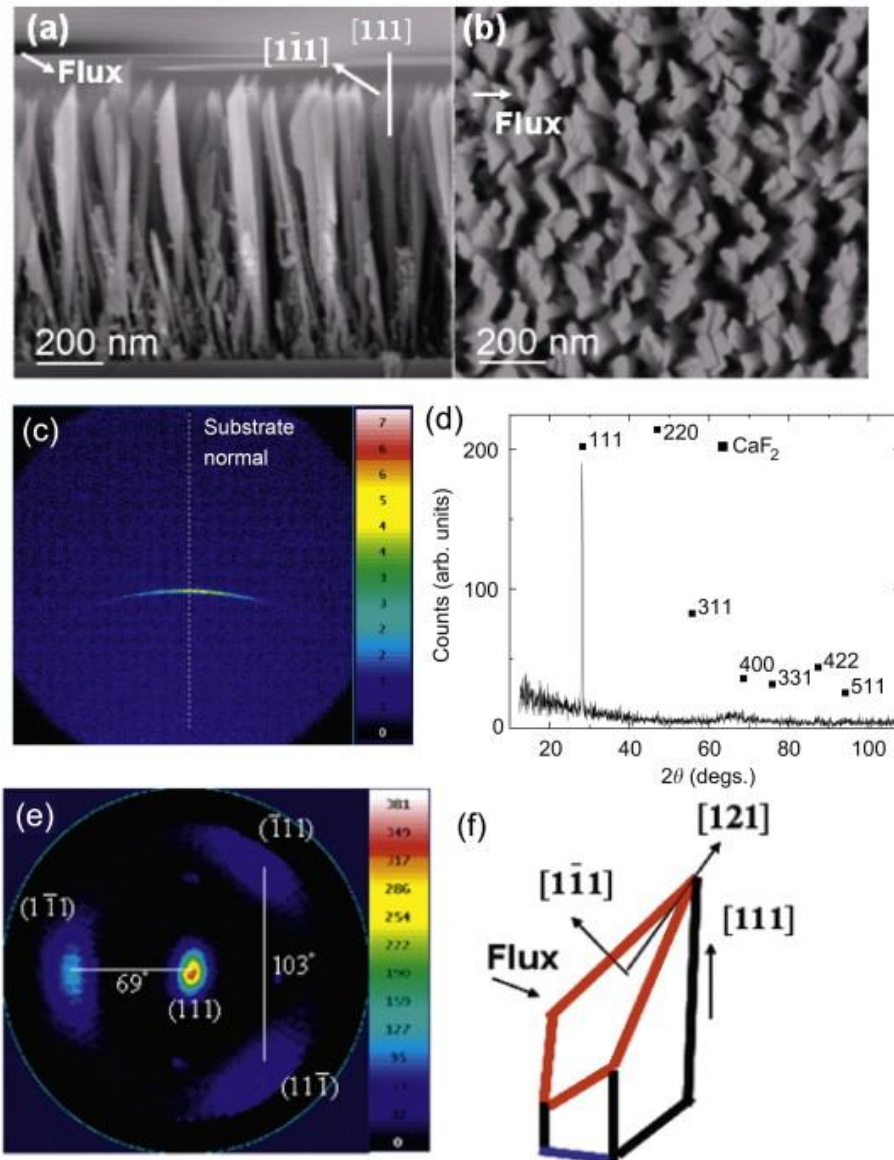
Fig 1.1: (a) SEM side view and (b) SEM top view of 750-nm-thick CaF2 nanorods grown by oblique angle (65°) vapor deposition incident from the left. (c) A two-dimensional (2D) X-ray diffraction pattern of the CaF2 nanorods film. (d) The 2θ plot constructed by integrating a narrow slice (±1°) of 2D diffraction patterns along the dashed line. (e) X-ray pole figure showing the [1 1 1] out-of-plane orientation of 750-nm-thick CaF2 nanorods. (f) A schematic showing the side view of a faceted CaF2 nanorod with the [1 1 1] direction perpendicular to the substrate, the [111] direction facing towards the incident flux, and the [1 2 1] direction in the facet plane.

(Credit: Li *et al.* with permission from The Journal of Crystal Growth)

Among these properties is the two-degree orientation of the nanorods which is a biaxial texture in which two crystallographic axes point in two preferred directions labeled as $<h_1k_1l_1>$ and $<h_2k_2l_2>$. The $<h_1k_1l_1>$ direction can be tilted away from the surface normal and the second direction, $<h_2k_2l_2>$ is an in plane preferred orientation.[6] For the case of calcium fluoride, which has a cubic structure, the lowest surface energy plane is (111).[6] For this reason, calcium fluoride nanorods form a large faceted surface facing the incident flux in the (111) plane. Through scanning electron microscopy, X-Ray diffraction, and X-ray pole figure analysis, the large faceted (111) out of plane orientation of these nanorods is shown in Fig. 1.1

The biaxial nature of these calcium fluoride nanorods has been demonstrated to have potential uses in the semiconductor (most specifically the solar cell semiconductor) thin film area as well as the superconducting thin film area due to its ability to serve as a buffer layer to grow quasi single crystal films on amorphous substrates.[7,8,9,10] One of the most noteworthy characteristics of calcium fluoride substrates (which also make them even more useful), is that they defy the general rules of crystal growth through shadowing techniques.[5] At oblique angles α less that 65°, these structures have a negative β angle. In essence, the rods lean away from the incident flux. For flux angles α greater than 65°, the rods tilt towards the incident flux.[5] In essence, these faceted tips can be angled in virtually any desirable direction from the substrate normal as opposed to most instances where the rods always grow toward incident flux. It has also been seen that at the nanoscale, these rods can still orient films with a large lattice mismatch due to their plastic deformation characteristics.[8] These nanorod arrays have been studied for

multiple applications where they serve as a buffer layer to grow films. This work differs in that it is focused on their ability to orient nanoparticles using the facets and geometries of the tips.

Chapter 2: Experimental Procedure

2.1 Experimental Setup

All samples were grown using a home made thermal deposition chamber shown and labeled in Fig. 2.1. This chamber uses a combination of a mechanical scroll pump, a turbo molecular pump, and if needed, a titanium sublimation pump to achieve the low base pressures required for sample growth and quality. The scroll pump operates on the principle of two scrolls (one fixed and one rotating eccentrically) to compress any air trapped between the two towards the desired direction. A diagram of the basic mechanics of this is shown in Fig. 2.2. This pump was used to achieve a pressure of approximately 1×10^{-2} Torr from atmosphere. At this pressure, the combination of the scroll pump and the turbo molecular pump were used to achieve a base pressure within the chamber of approximately 5×10^{-7} Torr. The turbo molecular pump uses a system or rotor/stator pairs to knock gas molecules into successively lower series until they are through the pump and exhaust. The rotor blades are angled in such a way that as they spin, they collide with entering gas molecules and transfer mechanical energy to them. The resultant momentum of the molecules sends them towards inlets in the stators at which point the process repeats itself. A diagram of the mechanics of this system is shown in Fig. 2.3.
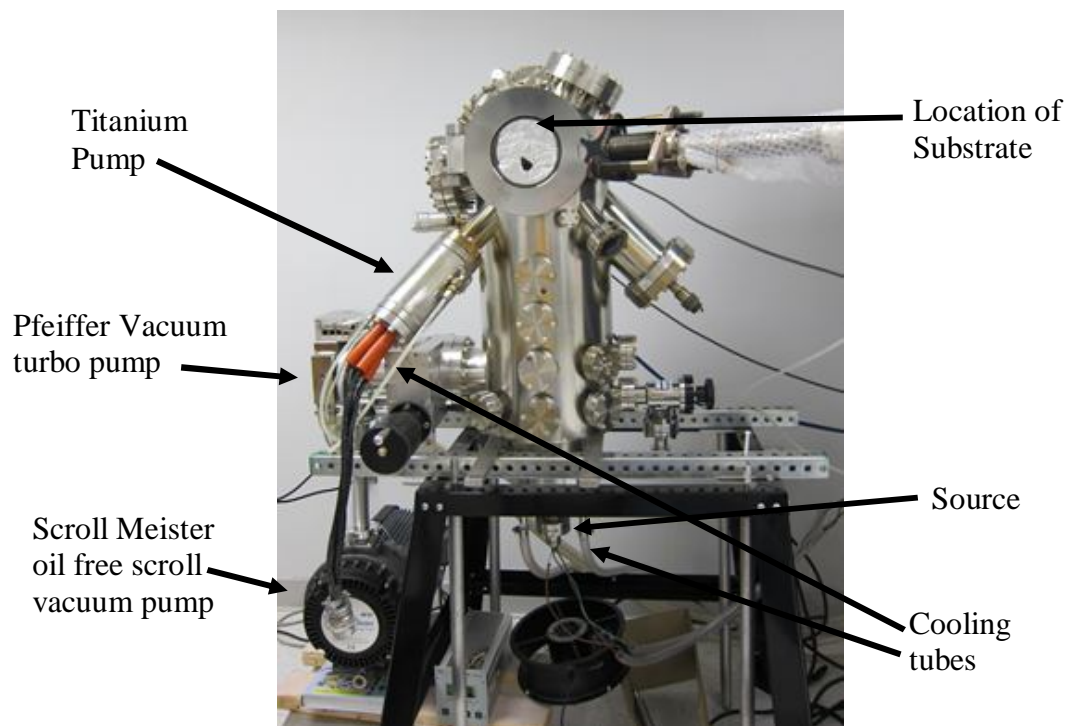
Fig. 2.1: Home made thermal atomic vapor deposition chamber
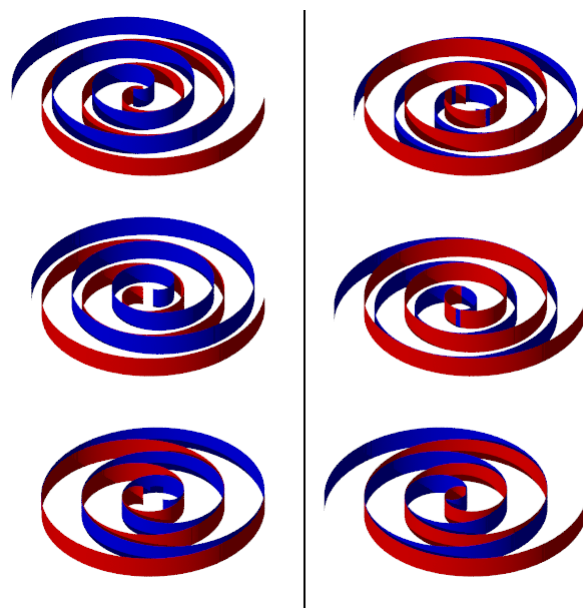
Fig. 2.2: Scroll Pump mechanism using Archimedean Spirals (Credit: Wikipedia)
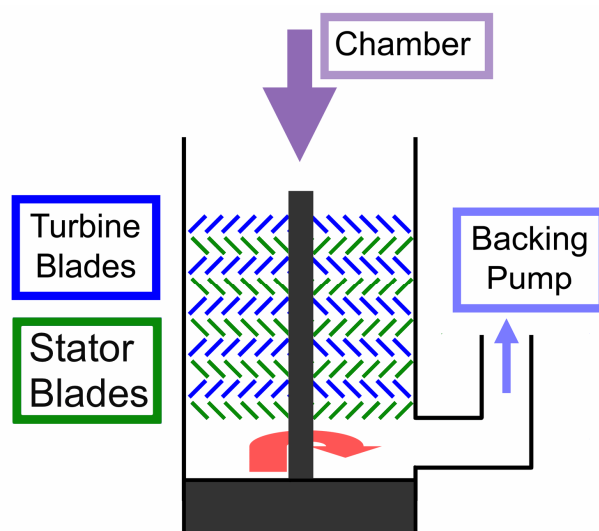
Fig. 2.3: Schematic of turbo molecular pump

(Credit: Wikipedia)

The desired base pressure was verified using an ionization gauge. With an ion gauge, a filament is heated to produce a regulated electron current. A positive voltage is then applied to a helical grid to attract the electron current. As the electrons move towards the grid, some of them collide with gas molecules causing them to be ionized. These molecules are then attracted to a central collector wire due to it having a negative voltage applied to it. A diagram of the basic operation of the ion gauge is shown in Fig. 2.4. When the desired base pressure is achieved, the sample is grown by heating a graphite crucible containing the source that we wish to deposit until the source evaporates into an atomic vapor. This is done by heating a tungsten filament surrounding the crucible to create an electron current and then directing the current towards the crucible

by applying a voltage bias, up to 1000V, between the two. The bombardment of electrons onto the crucible heats it to the necessary temperature.
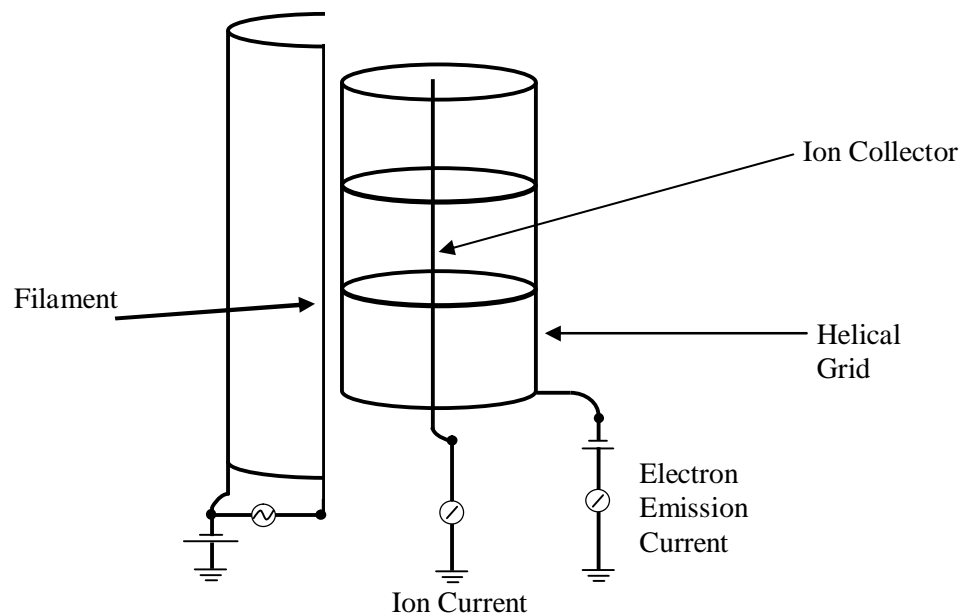
Fig 2.4: Schematic of an ionization gauge

2.2 Sample Growth

Calcium fluoride nanorods were first grown on silicon substrates using a thermal deposition chamber. As the atoms deposit on the silicon substrate, ad-atom diffusion causes them to find energetically favorable sites on the substrate.[11] By creating a large oblique angle between the substrate and the source, taller areas of the film will shadow lower areas blocking the atoms from reaching those parts of the substrate. This glancing

or oblique angle is the measurement between the substrate normal and the incident vapor flux. As the taller initial areas continue to collect atoms, they grow into nanorods. The substrate was placed at an oblique incident angle to the source to promote the growth of nanorods rather than thin films by using the shadowing effect to promote localized growth. In this instance, the calcium fluoride rods were grown on a substrate at an oblique angle $\alpha \sim 75°$. The substrate was silicon which was tilted to the desired oblique angle. The setup of this is shown in Fig. 2.5 with the effects of shadowing shown in Fig. 2.6. For these experiments, the thermal deposition chamber used operated at a base pressure of $\sim 5 \times 10^{-7}$ Torr. The majority of the vapor flux, due to the orientation and shape of the crucible, evaporated towards the substrate and was incident at the predetermined oblique angle.

Creating a large oblique angle between the deposition flux and the substrate, it is possible to grow nanorod arrays as opposed to a film due to the incident flux preferentially depositing on top of surface features with larger height values. Not only does this promote the growth of nanostructures rather than a uniform film, but it is also conducive to creating a formation of well separated nanostructures growing outward in the general direction of the incident flux. Typically the angle β of the nanostructures leaning towards the incident flux is a value that is smaller that the actual oblique angle α.[12] Calcium fluoride was chosen as the material for the nanostructures for several reasons, one of which is that it does not adhere to this rule. In the case of calcium fluoride, the value for the angle β can be negative or smaller compared to the incident angle α. In essence, the nanorods do not always incline towards the incident flux, but away from the flux as well depending on the incident angle. In addition to this, the

calcium fluoride nanorods have a characteristic biaxial tip with a large (111) facet facing the incident flux. This permits one to mimic growth on a single crystal substrate without going through the difficulties necessary to actually create a single crystal substrate. The rods were grown to an approximate length of 500 nanometers and a thickness of 20 nanometers.

Using the same deposition system, silver nanoparticles were then deposited onto the calcium fluoride nanostructure array. Initially, the substrate was placed at an angle normal to the source for this process. After scanning electron microscope (SEM) and transmission electron microscope (TEM) imaging showed that this caused the nanoparticles to have no real preference in where they adhered to the rods, the silver deposition was done with the substrate at the same $75°$ oblique angle to the source as when the calcium fluoride was deposited. SEM and TEM imaging of these samples showed that the silver nanoparticles preferentially and exclusively adhered to the large (111) facet of the calcium fluoride rod's biaxial tip. A representation of the calcium fluoride deposition along with the normal and oblique deposition of silver on the calcium fluoride rods is shown in Fig. 2.7.
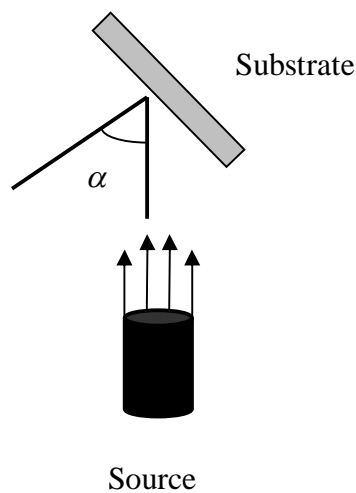
Fig. 2.5: Diagram of oblique angle deposition
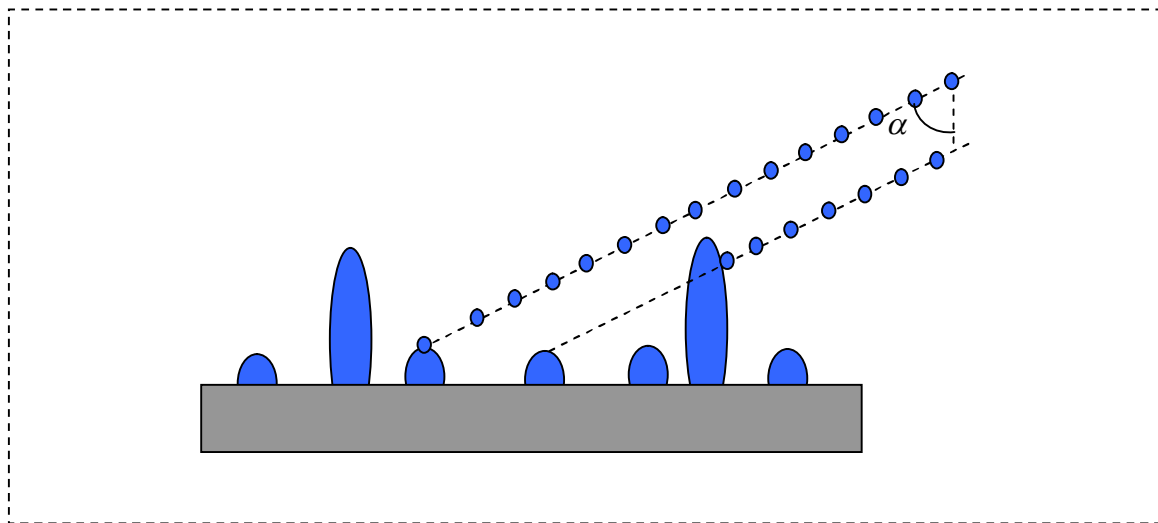
Fig. 2.6: The effect of shadowing during oblique angle deposition. Islands of the deposited material begin to nucleate at the surface. As they start to grow in height, the incident flux of material impinging on the surface at oblique angle α will preferentially deposit on the taller features which will in turn shadow the shorter islands preventing their continued growth.
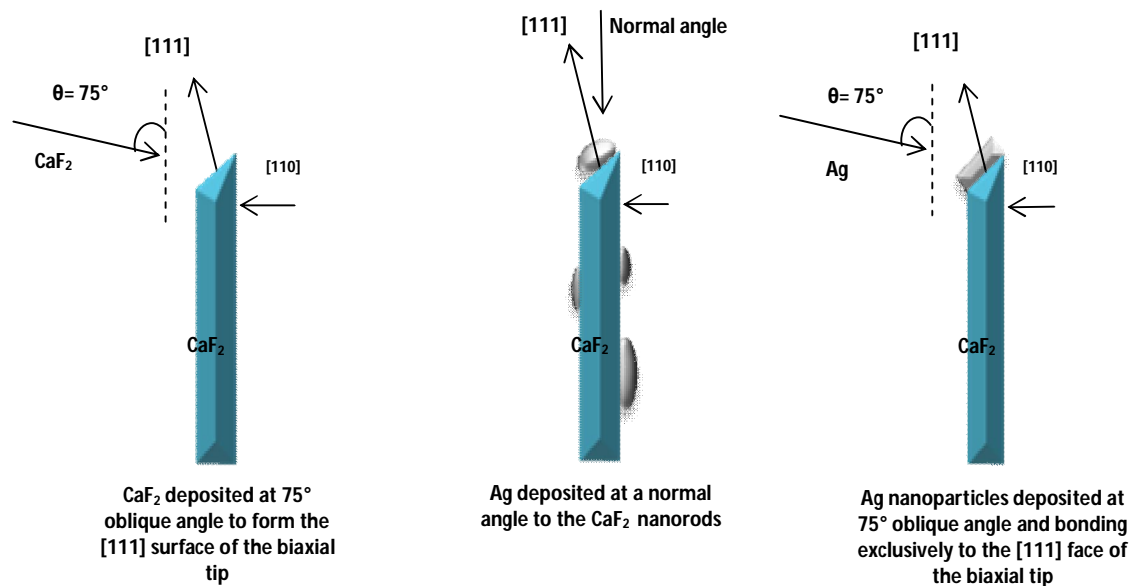
Fig. 2.7: Calcium fluoride deposition with flux angle shown in (a), silver deposition with angle normal to substrate (b), and silver deposition on calcium fluoride nanorods at oblique angle (c).

Chapter 3: Characterization

3.1 SEM Imaging

The samples were first characterized using a SEM. In this instance a Hitachi field emission FE-SEM Su-70 was used. A SEM uses a beam of electrons which is focused and condensed using magnetic lenses to scan a sample in a raster (rectangular) fashion to obtain information about its morphology and composition. The electron beam is emitted by heating an electron gun typically equipped with a tungsten or lanthanum-hexaboride filament. As the primary electron beam hits the sample, secondary electrons generated from the sample are scattered into collectors through in-elastic scattering between the beam electrons and the atoms in the sample.

All samples were sputtered with a small amount of platinum to increase their conductivity and reduce charge in the SEM to obtain better resolution in the images. Top view images were first taken of the samples. These images show dispersed calcium fluoride nanorods with silver nanoparticles adhering to the tops of the rods. The silver nanoparticles can also be seen to be progressively larger with the increasing growth thickness. Cross section images were then taken of each sample. The cross sectional images show the calcium fluoride rods to be tilted towards the incident flux at a smaller β angle than the initial oblique angle α of the substrate to the source. This angle

corresponds to results that have previously been published by other groups. The large (111) facet of the biaxial tips in the direction of the flux can be seen as well as the exclusive adhesion of the silver nanoparticles to that facet of the tip in each sample. The increasing diameter of the silver nanoparticles can also be observed with the increase of the growth thickness. The cross sectional and top view images of each sample are shown in Figs. 3.1, 3.2, and3.3. Figs. 3.1, 3.2, and 3.3, show progressively the top view and cross sectional views of the 5, 10, and 15 nanometer samples that were grown. The angles measured in all three samples using cross sectional imaging show a positive β angle of approximately 10° from the substrate normal with regards to an incoming incident flux angle α of 75° which corresponds to the results in the literature.
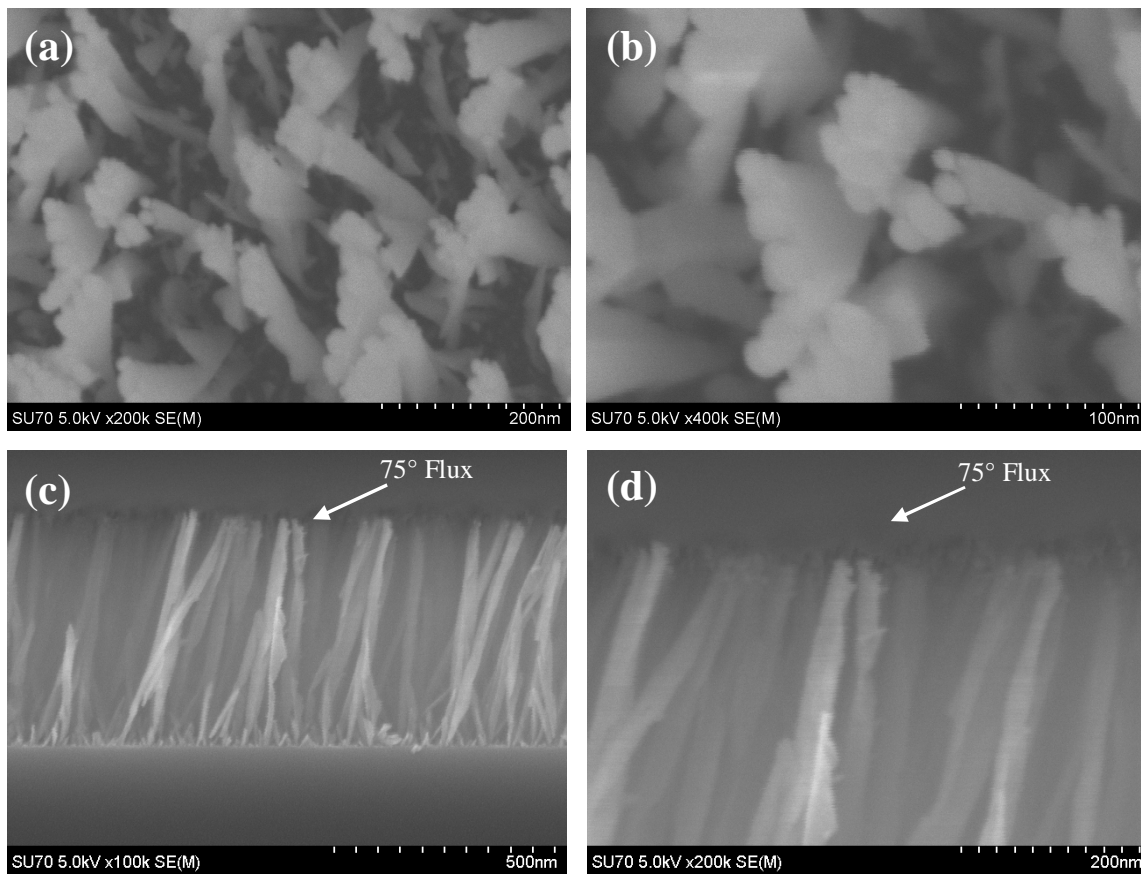
Fig 3.1: SEM images of the first sample grown with 5nm silver deposited on rods. Images (a) and (b) are top view showing beads deposited on large calcium fluoride tip facet. Images (c) and (d) show cross sectional views of nanostructures with negative angle from incident and beads exclusively adhered to the larger (111) facet.
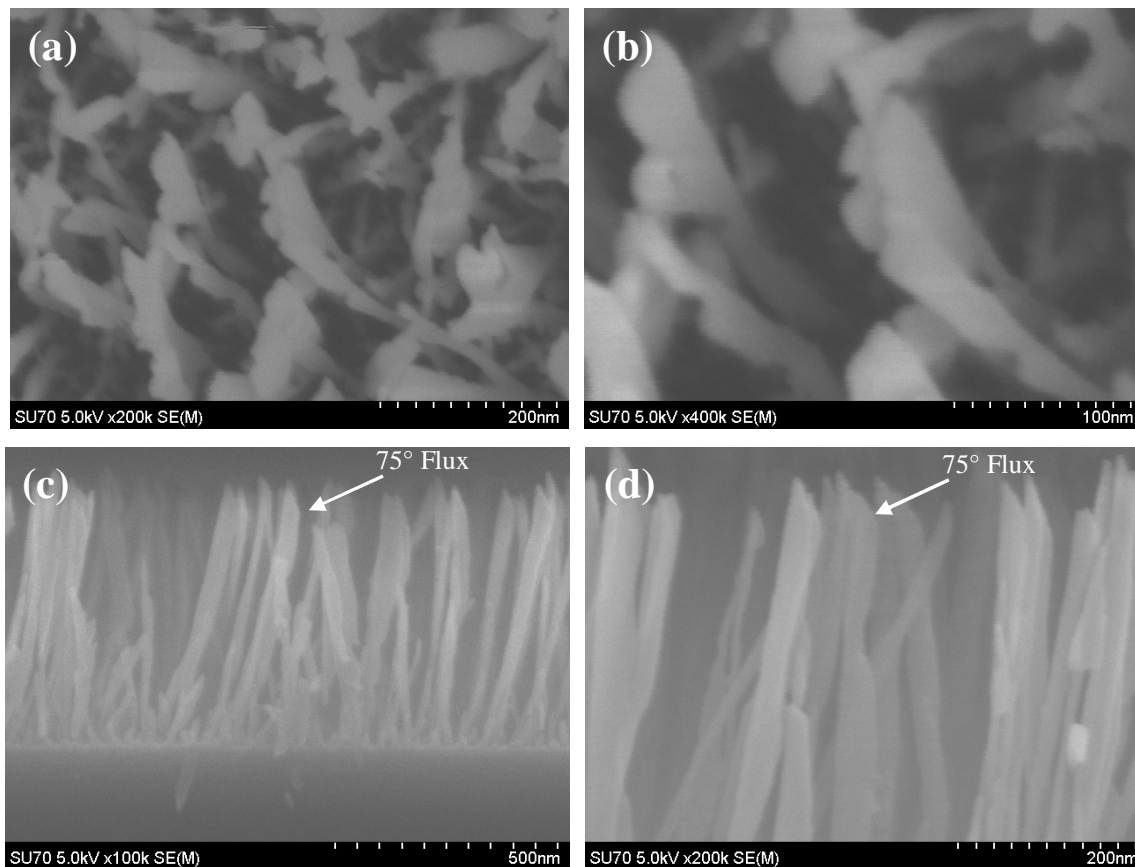
Fig 3.2: SEM images of the second sample grown with 10nm silver deposited on rods. Images (a) and (b) are top view showing beads deposited on large calcium fluoride tip facet. Images (c) and (d) show cross sectional views of nanostructures with negative angle from incident and beads exclusively adhered to the larger (111) facet
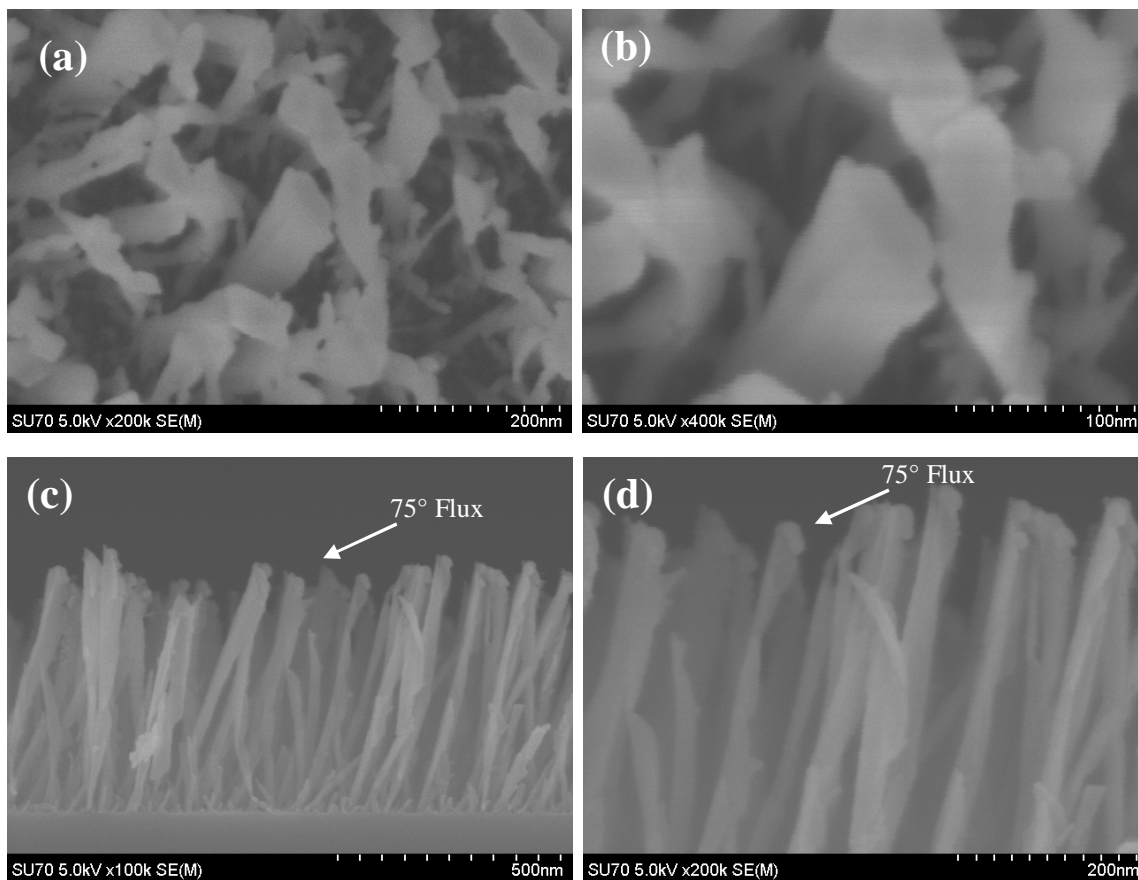
Fig 3.3: SEM images of the second sample grown with 10nm silver deposited on rods. Images (a) and (b) are top view showing beads deposited on large calcium fluoride tip facet. Images (c) and (d) show cross sectional views of nanostructures with negative angle from incident and beads exclusively adhered to the larger (111) facet

3.2 TEM Characterization

Bright field imaging, high resolution imaging, diffraction, and dark field imaging were used to characterize each sample using a Zeiss Libra 120KV TEM. A TEM works similarly to an SEM in that a gun at the top of the column emits a beam of electrons that are focused and condensed by magnetic lenses. There are however several key differences. The main difference is that instead of the electron beam or sample's electrons being reflected off the surface of the sample, a thinner piece of sample is placed on a mesh grid with a carbon film on it and the beam is transmitted through the sample. Different lenses and apertures are then used after the beam passes through the sample to condense it and manipulate it to high magnification and resolution images as well as other useful characterization techniques that permit elemental analysis as well as crystal orientation and geometry. In all characterization modes, the beam is first focused on a phosphorus screen at the bottom of the column and observed optically until a generally well focused result is attained. After this, the screens are raised and a charge coupled device (CCD) camera along with software is used to better focus and obtain the image, diffraction pattern, or spectrum that is desired.

With bright field imaging and high resolution imaging, the principles are similar to SEM imaging except that one is observing the resultant electrons passing through a sample. Since the electrons are passing through the sample, thinner pieces of the sample or areas where the sample is non-existent will appear brighter. Thicker pieces of the sample or elements that have a higher atomic number will appear darker as they allow fewer electrons to pass through. For diffraction, X-Ray diffraction (XRD) is what

typically comes to mind. Due to particle wave duality and their small wavelength, electrons can be thought of in this instance as a wave and can use the same laws and principles as XRD. From this, we can use Bragg diffraction to determine the lattice spacing and orientation of our crystal structures. To satisfy the Bragg condition, shown in Fig. 3.4, a beam of energy or electrons is incident on a crystal structure and is scattered with constructive interference by the atoms in the sample. Bragg's Law which is given as

$$n\lambda = 2d \sin \theta , \tag{6}$$

is the expression of this phenomenon where n is an integer, λ is the wavelength of the incident beam of particles or energy, and d is the inter-atomic spacing of the crystal lattice. In this instance, all materials in the sample are cubic so we can find the lattice spacing using the relation,

$$d = \frac{a}{\sqrt{h^2 + k^2 + l^2}} \tag{7}$$

for a lattice spacing a and Miller indices $h, k,$ and l. For electron beam diffraction, the beam interacts with both the electrons and the nuclei in the sample. The incident electron beam interacts with the electromagnetic fields of the sample and are directly scattered. [13]

In dark field imaging, diffraction is first taken of the sample, and the resultant desired spot or ring is examined. By centering in on the desired spot or location, it is possible to exclusively illuminate the parts of the sample corresponding to that scattered spot of electrons which are diffracting from a certain geometry in the sample itself. This can be used to verify which parts of a particular sample are responsible for causing that

particular diffraction pattern due to its geometry. This in turn, lets one see where in the sample, and how much of a sample, has the particular geometry and orientation that is being examined.
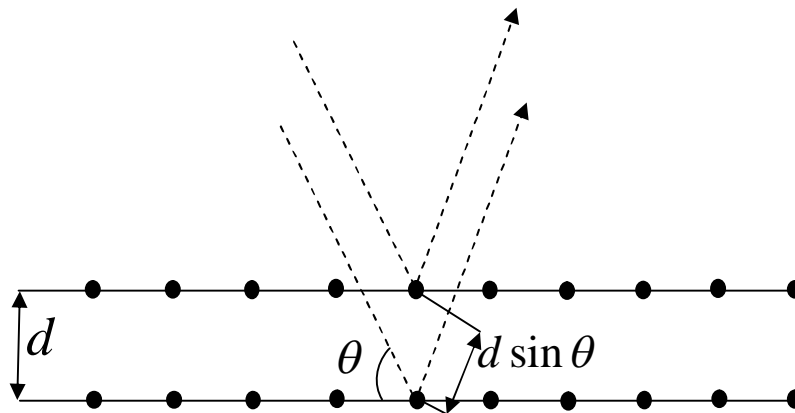
Fig. 3.4: Bragg diffraction. Beams with identical wavelengths and phases approach a crystalline solid and are scattered off two atoms within it. The second beam has an extra length of $2d \sin \theta$ and constructive interference occurs when the beams are integer multiples of the wavelength of the incident beam.

3.3 TEM Bright Field Imaging/High Resolution

Bright field imaging was done to re-confirm the exclusive growth and adhesion of the silver nanoparticles to the desired (111) facet of the calcium fluoride tip of each sample. The images re-confirmed the original SEM imaging with regards to exclusive growth and adhesion to the desired surface of the tip. The diameters were also measured

of silver nanoparticles for all three samples with sample images of average looking parts of each shown in Fig. 3.5 along with the measurements of their nanoparticles. The nanoparticles that were measured ranged in diameters of 3-8 nanometers for the 5 nanometer sample, 10-20 nanometers for the 10 nanometer sample, and 15-35 for the 15 nanometer sample. The diameter of the nanoparticles can be shown to scale in size with the deposition thickness of each sample, although they do not have the exact same thicknesses as the deposition target values. In each of the three samples, with example images shown in Fig. 3.5, observation shows this to be due to the nanoparticles beading up on the surface of the sample as opposed to growing as a film due to the large lattice mismatch between the calcium fluoride (111) (~3.15 Å in XRD database) lattice constant as opposed to silver (111) (~ 2.4 Å in XRD database). This can be attributed to Stranski-Krostanov crystal growth.[14] In this growth method, a film of no more than several mono-layers thick will grow at the interface. At a certain point, which is determined largely due to strain and chemical potential, a critical layer thickness will be achieved at which point the crystal growth will continue due to nucleation and coalescence of absorbate islands.[15,16,17,18] Because of this, the diameter of the beads on average is greater than the deposited thickness of the silver of each sample if it were grown as a film on an amorphous substrate. Through proof of epitaxy at the interface between the two materials (shown in chapter 3 section 4), we can know this growth method to be the Stranski-Krostanov method as opposed to the Volmer-Weber growth method where adatom-adatom interactions are stronger than adatom interactions with the surface, resulting in the growth of islands on the surface.[17]

Next, high resolution transmission electron microscopy (HRTEM) was taken of a calcium fluoride nanorod sample grown to the same approximate lengths and thicknesses as the nanorods which had the silver deposited on them. Using HRTEM, it was possible to see the lattice fringes of the sample at the tips of the nanorods, shown in (b) and (c) of Fig 3.6.Using both the images and the fast Fourier transform (FFT) of the images, shown in (d) of 3.6, it was possible to calculate the lattice spacing to be approximately 3.11 Å which confirmed the tip facet to be (111) in orientation. Due to the limitations of this particular transmission electron microscope, it was not possible to get a high enough resolution to confirm (111) orientation of the silver nanoparticles using this method. Dark field and diffraction were used instead to confirm that the silver nanoparticles did indeed grow at (111) orientation at the silver-calcium fluoride interface.
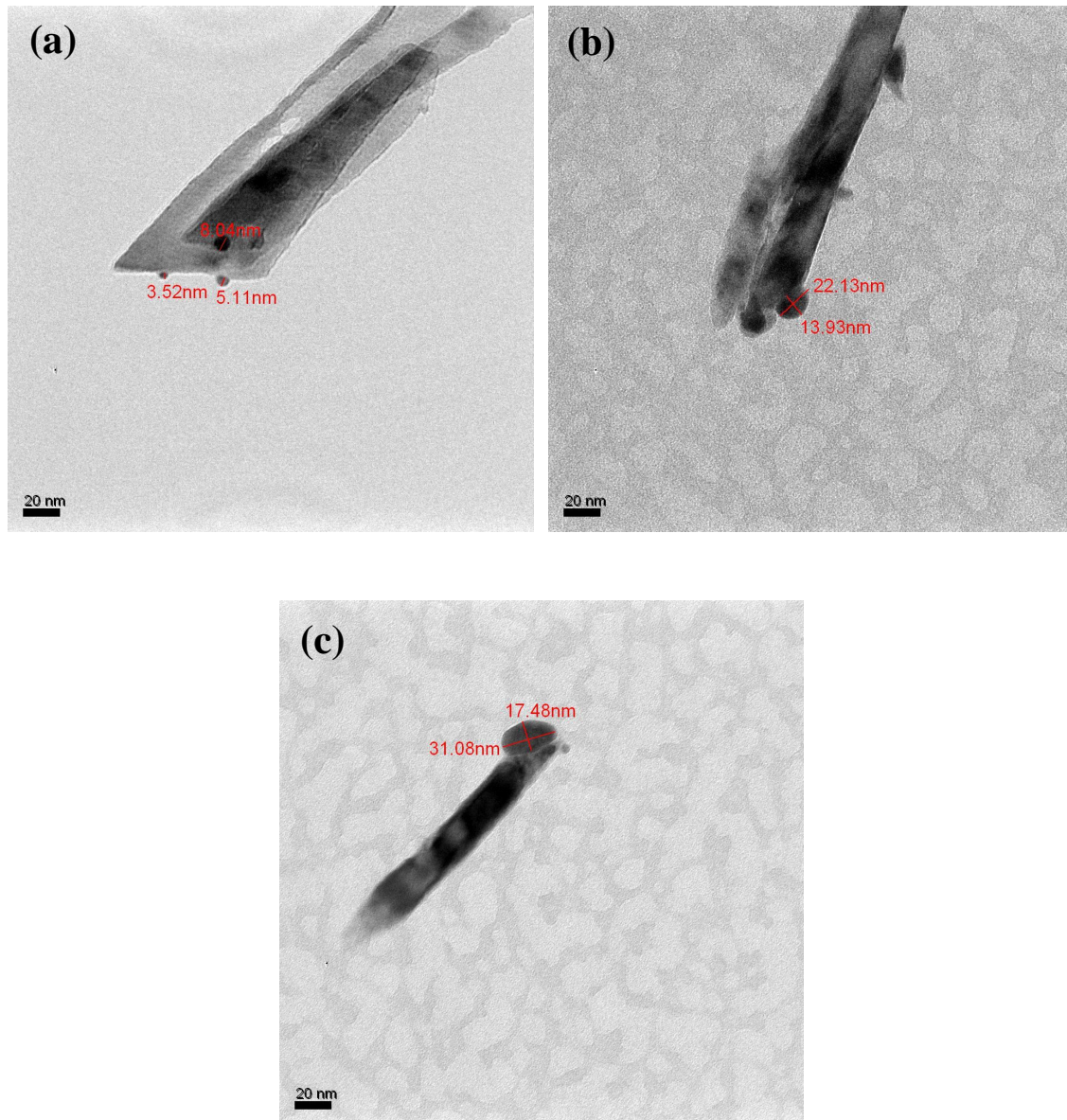
Fig 3.5: Annotated TEM bright field imaging of a rod from each sample grown. The 5nm annotated sample rod is shown in image (a) annotated 10nm sample rod in (b), and the annotated 15nm sample shown in (c).
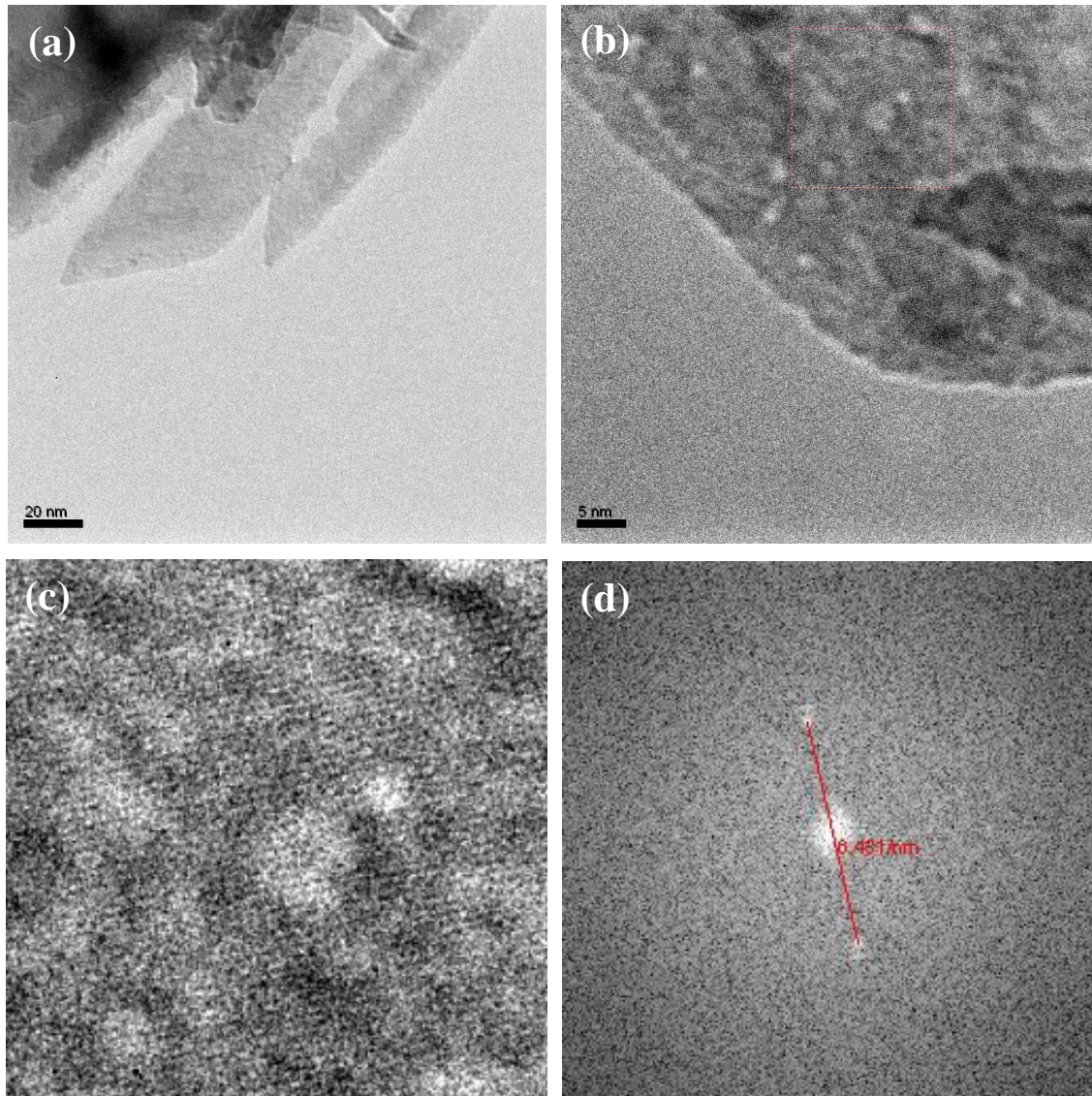
Fig 3.6: HRTEM and lattice fringes of calcium fluoride nanorod with the rod shown in (a), the high resolution shown in (b), the sampled fast Fourier transform (FFT) area of the lattice fringes in (c), and the FFT shown in (d)

3.4 Diffraction and Dark Field Imaging

To obtain the data to confirm (111) orientation of the silver nanoparticles at the interface along with re-confirming the (111) orientation of the calcium fluoride, diffraction was taken on each sample of each silver thickness. In order to obtain a diffraction pattern with enough points/rings to work with, larger portions of the sample were used in this part of the characterization as opposed to individual rods/beads. The diffraction rings were then measured and the lattice spacing was once again calculated for the calcium fluoride and calculated for the silver as well. The rings showed the calcium fluoride (111) lattice spacing to be compressed to approximately 2.99Å and the silver (111) lattice spacing to be strained to approximately 2.53 Å. This can be explained due to the large lattice mismatch of the two materials. As the silver was deposited onto the calcium fluoride, it caused both materials to attempt to reach a lattice spacing with less of a miss-match. Although this result is not entirely unexpected, it is worth noting the lattice compression of the calcium fluoride and the straining of the silver by approximately 5 percent in each instance respectively. The straining of the lattice spacing of the silver would be conducive to catalytic efforts as surface reactivity increases with lattice expansion. [19]

Once diffraction had been taken on the samples, the desired (111) diffraction spots and rings of calcium fluoride and silver were focused on by centering on them and then going back into image mode. Dark field imaging of the (111) of calcium fluoride once again confirmed the orientation of the rod at the facet. The Dark field images of the silver conclusively confirmed (111) orientation of the
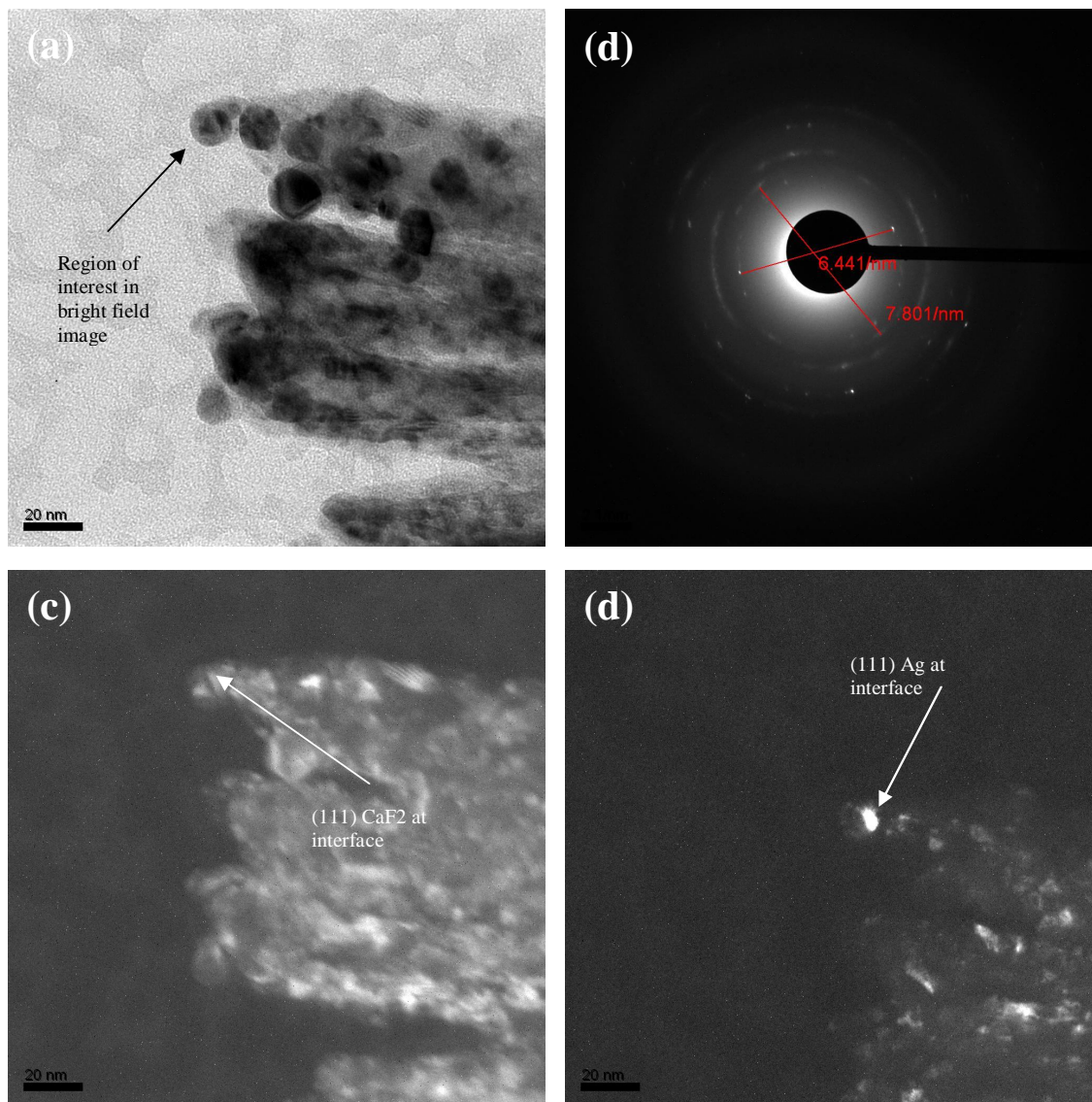
nanoparticles particularly at the interface. Dark field imaging also showed the 10nm sample to have nanoparticles with the most desired (111) composition. The 10nm sample exhibited the most abundant (111) orientation both at the interface and in the bulk of the particle. Bright field images, dark field images and diffraction patterns of each sample's rods and nanoparticles are shown in Figs. 3.7, 3.8, 3.9, and 3.10.

In Fig. 3.7 a bright field image is shown in (a) of the part of the 5 nanometer sample used. In (b), the diffraction rings with corresponding measurements are shown with the shorter being the (111) calcium fluoride and the longer being the (111) silver. The measurements of these diffraction rings along with the following three figures confirm that the lattice spacing of silver expanded by approximately five percent and the lattice spacing of calcium fluoride contracted by approximately five percent. In (c), dark field imaging was taken by using cone illumination of only the calcium fluoride (111) diffraction ring which shows (111) orientation at the interface. The illuminated parts of the sample are the parts that exhibit (111) orientation. In (d), dark field imaging was taken once again using cone illumination but this time of only the (111) silver diffraction ring. This shows that the silver did grow at the desired (111) orientation at the interface and in the bulk of the particle to an extent as well. Figs. 3.8 and 3.9 are a repetition of the process done in Fig. 3.7 but for the 10 nanometer sample. These two sets of images and diffraction patterns show far more illumination of the silver both at the interface and in the bulk of the particle for the (111) orientation than in the five nanometer sample leading to a conclusion that the 10 nanometer sample was a more ideal growth thickness for the desired result. Fig. 3.10 is once again a repetition of the previous processes but for the fifteen nanometer sample. It can be seen in these dark field images that almost no (111)

orientation is exhibited by the silver either at the interface or in the bulk of the particle which leads to a conclusion that the 15 nanometer sample is too thick to exhibit the desired result.
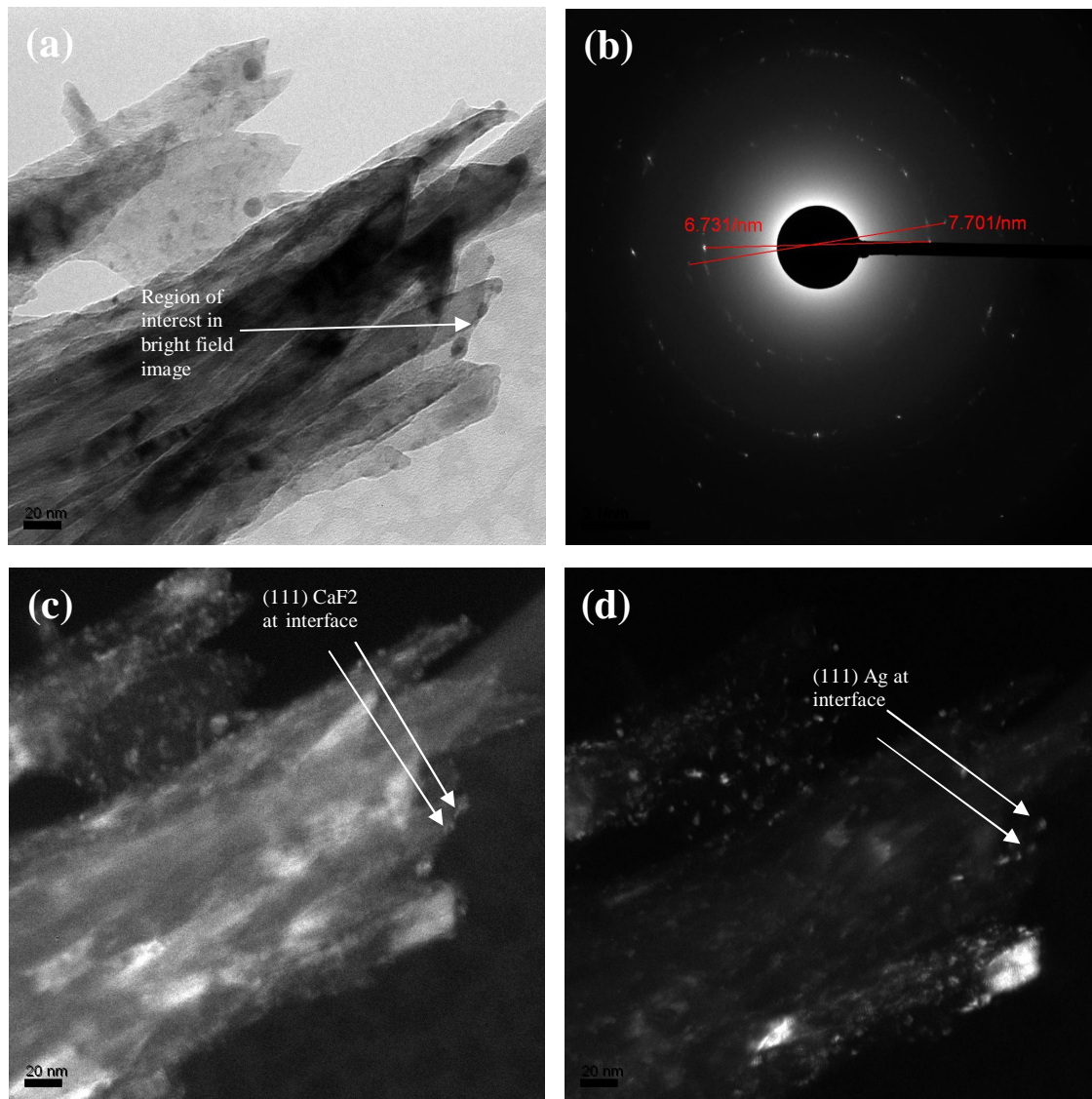
Fig 3.7: Image, diffraction pattern, and dark field of the 5nm sample. The image of the part of the sample diffraction was taken from is shown in (a), with the diffraction pattern and spacing shown in (b), the calcium fluoride dark field in (c), and the silver dark field in (d).

Fig 3.8: Image, diffraction pattern, and dark field of the 10nm sample demonstrating (111) orientation of the silver nanoparticles at the interface. The image of the part of the sample diffraction was taken from is shown in (a), with the diffraction pattern and spacing shown in (b), the calcium fluoride dark field in (c), and the silver dark field in (d).
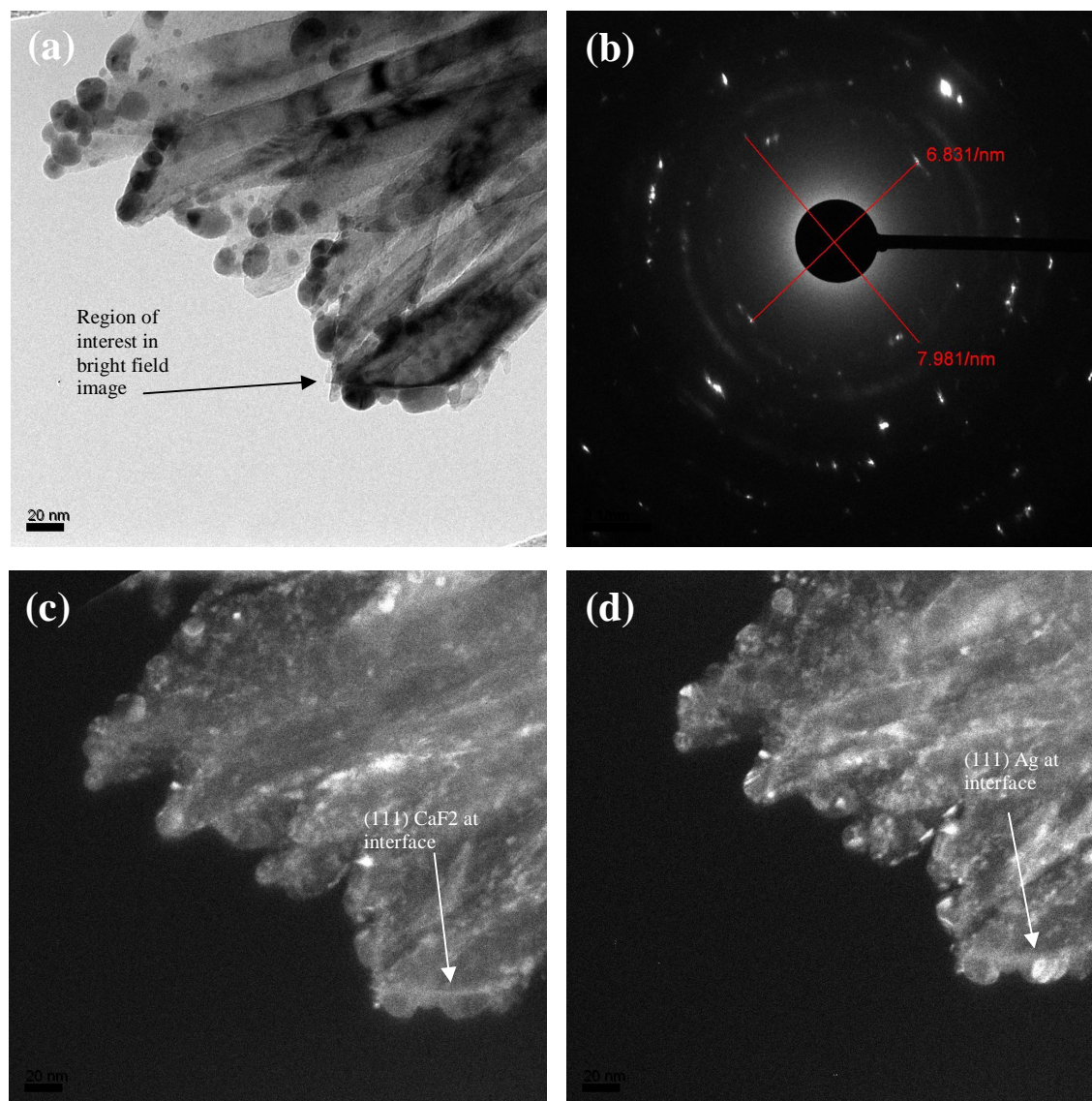
Fig 3.9: Image, diffraction pattern, and dark field of the 10nm sample demonstrating the overall (111) orientation of the silver nanoparticles. The image of the part of the sample diffraction was taken from is shown in (a), with the diffraction pattern and spacing shown in (b), the calcium fluoride dark field in (c), and the silver dark field in (d).

Fig 3.10: Image, diffraction pattern, and dark field of the 15nm sample demonstrating the overall (111) orientation of the silver nanoparticles. The image of the part of the sample diffraction was taken from is shown in (a), with the diffraction pattern and spacing shown in (b), the calcium fluoride dark field in (c), and the silver dark field in (d).
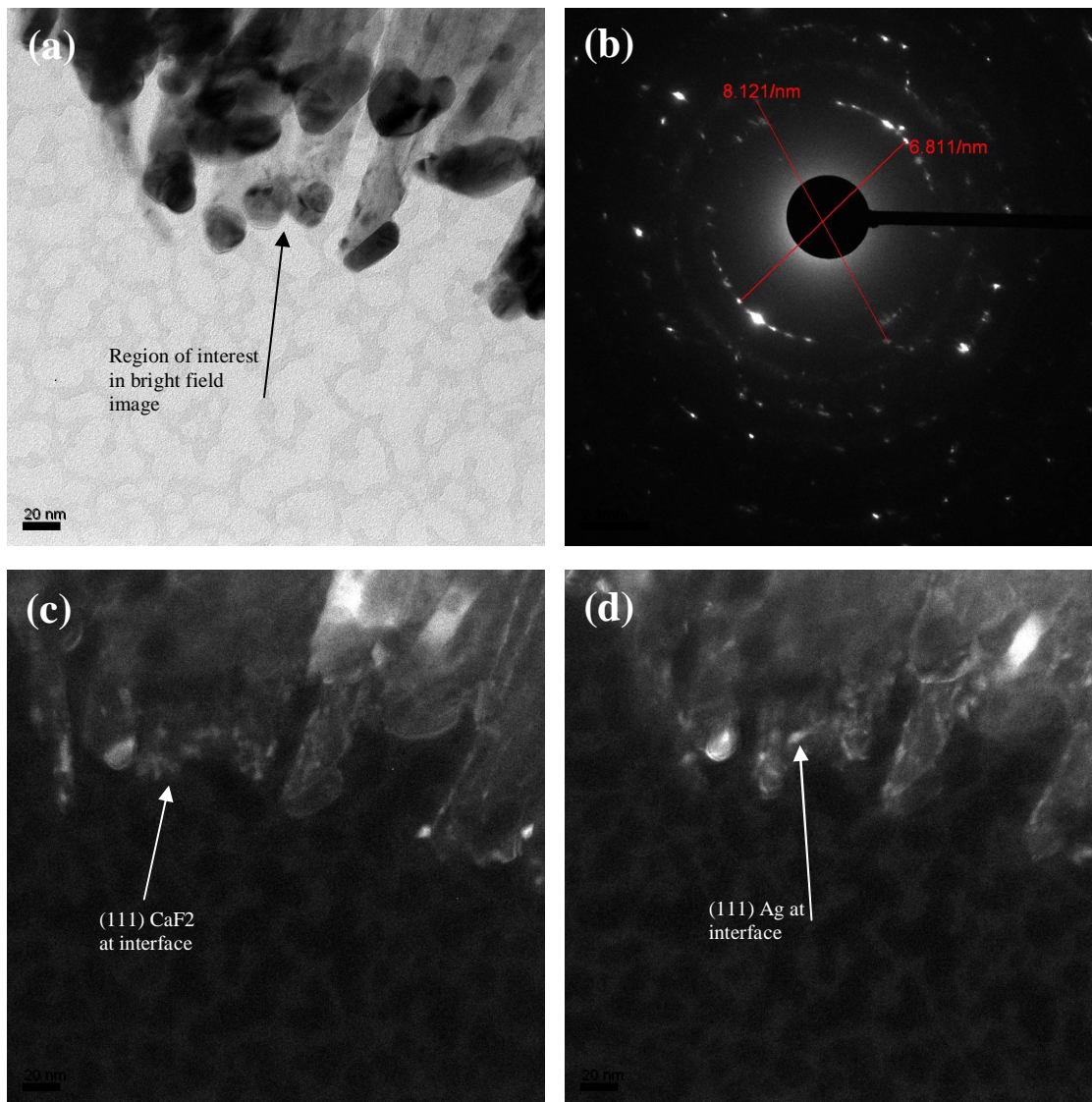
Chapter 4: Conclusions and Future Work

Silver nanoparticles were grown on a substrate of calcium fluoride nanorods in order to study preferentially orienting the geometry of metal nanoparticles for the purpose of catalysis. Both the nanoparticles and nanorods were grown using an oblique angle deposition technique in a thermal deposition chamber. The samples differed only in the angle of the substrate to the silver source and the thickness of the silver deposited once the angle was fixed. It was first demonstrated that it was possible to grow calcium fluoride nanorods with a large (111) facet on one side of their tips. It was then shown that it was possible to deposit silver nanoparticles exclusively on only one facet (the larger (111) facet) of the tip of the nanorods and only on the tip. It was furthermore demonstrated that it was possible to grow the silver nanoparticles with the desired (111) orientation at the calcium fluoride-silver interface with a silver thickness of 10 nm appearing to be the most ideal from the characterization done with regards to what percentage of the nanoparticles exhibited the desired geometry as well as at the interface. It was also demonstrated that the larger lattice spacing of the calcium fluoride made it possible to strain the lattice spacing of the silver in the (111) orientation.

A technique has been demonstrated to grow silver nanoparticles with a preferential (111) geometry at their substrate's interface despite a large lattice miss-match between the substrate and the silver which would prevent typical forms of orienting the particles using a substrate. It was also shown that this was possible to do without external

control of the temperature of the substrate. Further work on this project could include the examination and testing of these structures for their catalytic properties as well as examining the effects of the characteristics of the silver nanoparticles with the strained lattice. Following this, it would be worthwhile to examine if other metal nanoparticles exhibit the same behavior when deposited on these calcium fluoride substrates and to see if other nanorods with different tip geometries would make it possible to grow nanoparticles with the correspondingly different geometries at the interface. It would also be worthwhile to have the samples characterized in a superior TEM to attempt to obtain the lattice fringes at the interface and throughout the silver nanoparticles to show more conclusively which parts and how much of the nanoparticles exhibited the desired orientation.

References

[1] Catalysis. (2012, March 18). In Wikipedia, The Free Encyclopedia. Retrieved February

[2] J.M. Thomas, W.J. Thomas (EDs.), Principles and Practice of Heterogeneous Catalysis, VCH, Weinheim, 1997.

[3] Beatriz Roldan Cuenya, Synthesis and catalytic properties of metal nanoparticles: Size, shape, support, composition, and oxidation state effects, Thin Solid Films, Volume 518, Issue 12, 2 April 2010

[4] Somorjai, Gabor A., and Jeong Y. Park. "Colloid Science of Metal Nanoparticle Catalysts in 2D and 3D Structures. Challenges of Nucleation, Growth, Composition, Particle Shape, Size Control and Their Influence on Activity and Selectivity." *Springer Science+Business Media*. 2008

[5] Gaire, C., T-L Chan, Y. Liu, P. Snow, W. Yuan, M. Riley, G-C Wang, S. B. Zhang, and T-M Lu. "Calcium Fluoride Nanorods Defy Crystal Growth Rule." *NanotechWeb.org* (2010). *Nanotechweb.org Homepage*. Web. 12 Apr. 2012. http://nanotechweb.org/cws/article/lab/44148

[6] Lu, Toh-Ming, Fu Tang, and Gwo-Ching Wang. "Calcium Fluoride Nanorods Defy Crystal Growth Rule." *Invited Paper* (2008). *Nanotechweb.org Homepage*. RPI. Web. 12 Apr. 2012. <http://homepages.rpi.edu/~wangg/publications/shadowing%20growth%20of%20biaxial%20textured%20nanostructures%20films_SPIE.pdf>.

[7] H.-F. Li, T. Parker, F. Tang, G.-C. Wang, T.-M. Lu, S. Lee, Biaxially oriented CaF2 films on amorphous substrates, Journal of Crystal Growth, Volume 310, Issue 15, 15 July 2008, Pages 3610-3614, ISSN 0022-0248, 10.1016/j.jcrysgro.2008.04.040. (http://www.sciencedirect.com/science/article/pii/S0022024808003394)

[8] Toh-Ming Lu, Huafang Li, Churamani Gaire, Nicholas LiCausi, Tzu Liang Chan, Ishwara Bhat, Shengbai Zhang and Gwo Ching Wang (2010). Quasi-single Crystal Semiconductors on Glass Substrates Through Biaxially Oriented Buffer Layers. MRS Proceedings, 1268 , 1268-EE03-06 doi:10.1557/PROC-1268-EE03-06

[9] Licausi, Nicholas, Wen Yuan, Fu Tang, Thomas Parker, Huafang Li, Gwo-Ching Wang, Toh-Ming Lu, and Ishwara Bhat. "Growth of CdTe Films on Amorphous Substrates Using CaF2 Nanorods as a Buffer Layer." *SpringerLink*. Springer Science+Business Media, 8 Nov. 2008. Web. 12 Apr. 2012. <http://www.springerlink.com/content/l7j0617177765772/>.

[10] D. Han, H. Li, T.M. Lu and A.J. Steckl (2011). Unidirectional self-patterning of CaF2 nanorod arrays using capillary pressure. Journal of Materials Research, 26 , pp 223-229 doi:10.1557/jmr.2010.24

[11] J.G. Fan, X.J. Tang and Y.P. Zhao, Nanotechnology **15**, 501 (2004)

[12] D.-X. Ye, Y.-P. Zhao, G.-R. Yang, Y.-G. Zhao, G.-C. Wang, and T.-M. Lu, "Manipulating the column tilt angles of nanocolumnar films by glancing-angle deposition", Nanotechnology 13, 615-618 (2002)

[13] Williams, David Bernard., and C. Barry. Carter. *Transmission Electron Microscopy: A Textbook for Materials Science*. New York: Springer, 2009. Print.

[14] Stranski–Krastanov growth. (2012, March 18). In Wikipedia, The Free Encyclopedia. Retrieved February

[15] Venables, John (2000). *Introduction to Surface and Thin Film Processes*. Cambridge: Cambridge University Press. ISBN 0-521-62460-6.

[16] Pimpinelli, Alberto; Jacques Villain (1998). *Physics of Crystal Growth*. Cambridge: Cambridge University Press. ISBN 0-521-55198-6.

[17] Oura, K.; V.G. Lifshits, A.A. Saranin, A.V. Zotov, and M. Katayama (2003). *Surface Science: An Introduction*. Berlin: Springer. ISBN 3-540-00545-5.

[18] Eaglesham, D.J.; M. Cerullo (April 1990). "Dislocation-free Stranski-Krastanow growth of Ge on Si(100)". *Physical Review Letters* **64** (16): 1943–1946. Bibcode 1990PhRvL..64.1943E. doi:10.1103/PhysRevLett.64.1943

[19] Mavrikakis, M., B. Hammer, and J.K. Norskov. "Effect of Strain on the Reactivity of Metal Surfaces." *Phys. Rev. Lett. 81, 2819 (1998):*. 15 May 1998. Web. 12 Apr. 2012. <http://prl.aps.org/abstract/PRL/v81/i13/p2819_1>.